TRANSVERSE HARDNESS PHOTOTHERMAL PHASE IMAGING AND DEPTH-PROFILOMETRY OF HEAT TREATED STEELS

Y.Liu, A. Mandelis, N. Baddour, C. H. Wang,
Center for Advanced Diffusion-Wave Technologies, Department of Mechanical and Industrial Engineering, University of Toronto, Toronto M5S 3G8, Canada

Abstract: A method to image near-surface hardness profiles of heat-treated case-hardened steels using laser infrared photothermal radiometric phase imaging is described. It is shown that thermophysical and mechanical transverse inhomogeneity profiles in industrial case hardened steel samples are well correlated. Phase surface scanning imaging leads to a practical criterion for assessing transverse hardness homogeneity. A simple method based on phase imaging is proposed as a quantitative criterion to determine which steel samples should be rejected for thermal-wave depth-profilometric reconstruction of thermal diffusivity. Having developed this lateral hardness homogeneity criterion, we selected laterally homogeneous case-hardened industrial steels for thermal-wave frequency scans in order to perform depth profilometry of their thermal diffusivity. The reconstructed thermal diffusivity depth profiles from the samples were compared to the results of microhardness testing after each step of heat treatment: carbonitriding and quenching. The comparison showed that there is a good to excellent anti-correlation between hardness and thermal diffusivity profiles for both carbonitrided and quenched samples with 0.02" case depth and gradually worsening anti-correlation trends for 0.04" and 0.06" case depths.

Introduction: Thermophysical depth profilometry is a thermal-wave inverse-problem technique where thermal diffusivity profiles of a material are reconstructed from experimental surface data. Specifically for steels, since the thermal diffusivity depends, among other things, on their microstructural properties, monitoring this parameter indirectly gives information on changes that take place as a result of surface or bulk modification processes. In particular, thermophysical depth profilometry as implemented by laser photothermal means, has shown promise as a non-destructive alternative to existing costly, time-consuming and destructive techniques to determine metallurgical properties of case-treated steels.

Various independent groups of researchers [1-6] have studied the by now well-established anti-correlation between thermal diffusivity and microhardness. Only very recently have attempts been made to offer physical interpretations of photothermally reconstructed hardness depth profiles in processed steels. Nicolaides et al. [7] sought to understand the mechanism by which the thermal diffusivity profiles in carburized and hardened AISI 8620 steel arises. In the work of Nicolaides et al., a set of 8620 steel samples were studied after carburizing, followed by quenching. These two steps are normally performed sequentially to produce a quenched, hardened steel but were studied independently so that the origins of the thermal diffusivity profiles could be understood in detail. That study concluded that the depth distribution of the thermal diffusivity profile is dominated by carbon diffusion during carburization, while the absolute thermal diffusivity values are dominated by microstructural changes that occur during quenching. The authors also pointed out that the validity of these conclusions for other types of steel is uncertain. In order to address this issue of the more general validity of the foregoing conclusions, a similar study was performed on AISI 1018 steel and is reported here. While 8620 steel is typically carburized and then quenched in the process of case-hardening, 1018 steel is typically carbonitrided and then quenched.

During the heat-treating process, it is possible that a particular sample develops undesired lateral (transverse) hardness inhomogeneities, in addition to the desired depth inhomogeneity. Transversely inhomogeneous case hardened samples are not suitable candidates for the one-dimensional thermal-diffusivity reconstruction since the theory upon which the algorithm is based assumes that the inhomogeneity is in the depth direction only. Therefore, it is necessary to select only transversely homogeneous samples for reconstruction. Non-destructive evaluation should be introduced for sample selection. Much work has been done on the non-destructive evaluation of metals using thermal waves. The field of non-destructive evaluation with thermal waves has been

reviewed by Busse [8]. In another review, Busse and Walther reviewed the photothermal nondestructive evaluation of various materials [9]. In particular, thermal waves have been used to determine the depth of structures in metals, for the detection of faults and also for determining thicknesses and properties of hardened layers. Jaarinen et al. [10] determined the variation of thermal diffusivity with depth. For metals, the evaluations appear to be limited to detection of areas of prior deformation, fault inspection, profile analysis of seams and depth profiling. It was also shown that photoacoustic phase angle scanning can be used to measure subsurface structure in metals [11]. Associated with the foregoing depth-profilometric aspects of AISI 1018 steel, a method of transverse depth-profilometric hardness photothermal phase imaging and line scan to select the relatively homogeneous samples are introduced in this paper. The use of thermal waves to investigate various properties of metals is not new, however, the present imaging method to investigate the degree of transverse hardness homogeneity in a metal and to use it as a criterion to define thermomechanical homogeneity does not appear to have been previously considered.

Results: I. Sample preparation: Cylindrical samples one inch in diameter and 1 cm thick were cut from a bar of AISI 1018 steel. The chemical composition of this steel is 0.15-0.2% C and 0.6-0.9% Mn. The surfaces of the samples were ground with a 44, 54, 60 grit sand-wheel. The samples were subsequently carbonitrided and thermally quenched. The samples were treated in a Surface Combustion Super 30 Allcase Furnace, equipped with a top cool chamber for slow cooling processes. For the carbonitriding process, a base atmosphere consisting of nitrogen and methanol was used. The aim was to produce a nominal carrier gas composition consisting of 40% nitrogen, 40% hydrogen and 20% CO. To this base atmosphere an addition of enriching methane (CH4) and ammonia (NH3) gas was used. The ammonia was present throughout the entire cycle. The furnace was already conditioned (i.e. ammonia and methane and base atmosphere was set) before the samples were introduced. Flow scopes were used to set and control the ammonia and natural gas (methane) flows. Controlling the cycling time and temperature, we made 3 sets of samples with 0.02", 0.04" and 0.06" case depths.

II. Transverse hardness phase imaging and sample selection: As we mentioned above, transversely inhomogeneous samples caused by heat treatment are not suitable candidates for thermal diffusivity reconstruction. Therefore, it was necessary to perform the sample selections before the reconstruction. Phase imaging and line scans were performed for sample selection. The experimental set-up for photothermal radiometric (PTR) hardness imaging is shown in Figure 1. It consists of a high-power semiconductor laser the output of which is current-modulated, $I(\omega)$. The beam is expanded, collimated and then focused onto the surface of the sample with a spot-size of 1 mm. The harmonically modulated infrared (Planck) radiation from the optically excited sample surface is collected and collimated by two off-axis paraboloidal mirrors and then focused onto a HgCdTe detector. The signal from the detector is amplified by a low-noise preamplifier and then sent to a lock-in amplifier which is interfaced with a PC.

A photograph of a carbonitrided 1018 steel sample is shown in Figure 2. It is clear from the photograph that the surface of this particular sample contains some non-uniformities in color. These optical non-uniformities were generated at locations which were in contact with the basket supporting the steel samples during the furnace processing cycle. Therefore, the question arises as to whether this inhomogeneity is purely optical (confined to the surface) or if it represents hardness inhomogeneities at greater depths. To this end, the surface of the sample was scanned at 10 Hz using infrared photothermal radiometry. The results were mapped and are shown in Figure 3. Since the amplitude of the signal is proportional to (1-R) where R is the surface reflectance [12], variations in the signal amplitude over the sample surface resemble the shape of the discolored region of Figure 2. However, alongside the variation in signal amplitude over the sample surface there is a variation in signal phase as well. The photothermal phase is independent of the factor (1-R) [9] and thus is independent of the optical properties of the surface. The contrast in the phase scan of Figure 3 suggests the possibility of thermophysical and/or mechanical inhomogeneities across the sample.

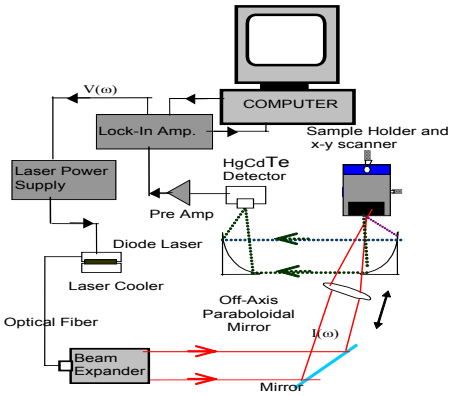

Figure 1 Experimental setup

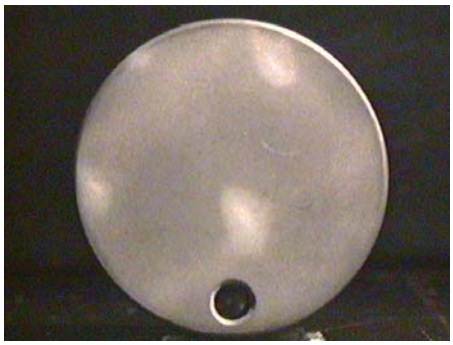

Figure 2 Example of a nonhomogeneous AISI 1018 steel sample and boundaries of PTR mapping range.

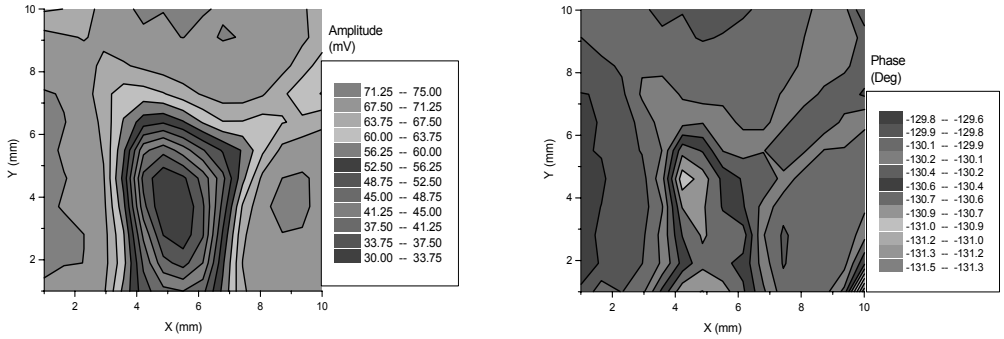

Figure 3. PTR surface maps of framed area in Figure 2 with 10 Hz modulated beam (nonhomogeneous sample).

Over a range of phase angles, the exact relationship between surface value of the thermal wave field and thermal diffusivity,α, for a homogeneous semi-infinite solid is given by

$$T(\alpha;\omega_0)=\int_0^{\infty}\frac{1}{\sqrt{\lambda^2+\sigma^2}}e^{-\frac{\lambda^2 d^2}{4}}\lambda d\lambda \qquad (1)$$

where $\sigma^2 = i\omega_0/\alpha$, ω_0 is a fixed angular frequency and d is the diameter of the beam, [13]. Since T is a complex number, we only consider the phase dependence on α. However, for a small range of phases such as those found in the phase maps, the relationship between the phase of T and thermal diffusivity, α, can be accurately represented as being linear; $\arg\{T(\alpha;\omega_0)\} = c_1\alpha + c_2$, where c1 and c2 can be found by a simple linear fitting. This is accomplished by plotting the phase of equation (1), given a particular frequency and beam size, against a small range of thermal diffusivity centered around a chosen reference thermal diffusivity value. In this work, the measured value of thermal diffusivity of the bulk was used. The linearity can be exploited to quickly determine the change in average thermal diffusivity across the surface of a sample. At the chosen points, this gives a measure of the mean thermal diffusivity within a thermal diffusion length. A surface map of average thermal diffusivity of the sample in Figure (3) is shown in Figure (4). A change in the chosen reference thermal-diffusivity

value will change the absolute thermal-diffusivity values as given in Figure (4) but will preserve the relative changes in thermal diffusivity.

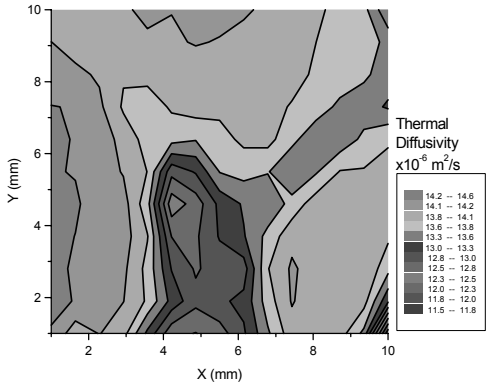

Figure 4. Average thermal diffusivity surface map of framed area in Figure 2.

For comparison purposes, a similar phase/amplitude mapping was performed on a visually homogeneous sample and is presented in Figure 5. From the very small signal (amplitude and phase) variations across this map, the homogeneity of the sample is obvious. Figures 6 and 7 show additional surface scans performed on yet another sample. This sample is made of AISI 8620 steel, carburized and quenched in a heat-treatment similar to that for the 1018 steel. This sample is inhomogeneous and this can be seen quite well in the phase mappings performed at both 10 Hz and 1 kHz. It should be noted that low-frequency phase variations of up to 2° constitute severe near-surface thermophysical inhomogeneity and possibly strong hardness inhomogeneity, Figs 3, 6, and 7, whereas phase variations of less than 0.5° are benchmarks of a thermophysically and possibly mechanically homogeneous sample, Figure 5. Figures 6 and 7 show that amplitude scans are dominated by changes in optical reflectance and thus images obtained at different frequencies vary little. On the other hand, phase images can vary significantly as they are dominated by thermophysical properties within depths on the order of the thermal diffusion length. Although optical inhomogeneities (amplitude images) can be indicators of thermomechanical inhomogeneities (phase images) as in Figure 3, this is not always the case (e.g. Figures 6 and 7).

To illustrate the foregoing observations and correlate mechanical and thermal-wave image profiles, PTR radial line-scans were performed on a fixed radius of the sample of Figure 2 at three different frequencies, 10 Hz, 100 Hz and 1000 Hz. At each frequency, a 1 mm-size beam was employed and measurements were made at eight different points across the radius indicated by dashed lines in Figure 2. The PTR amplitude and phase signal results are shown in Figure 8. The shape of the signal amplitude across the scanned diameter remains essentially the same for the three frequencies, an indication that the surface optical reflectance dominates the PTR amplitude. However, the shape of the signal phase changes with frequency and thus points to changing thermal properties of the sample across the transverse scan. The implication here is that PTR phase imaging such as shown in Figs. 3, 6 and 7 is capable of yielding sub-surface depth profilometric hardness images at different frequencies.

To demonstrate this claim, the corresponding surface microhardness tests of the same sample were made along the dashed line of Fig. 2 with an indenter and are presented in Fig. 9, confirming that the chosen sample does indeed contain a transverse inhomogeneity. In particular, there is a clear correlation between the diameter hardness test performed with a 1 kg load, Fig. 9a (which thus indents deeper into the steel) and the phase portion

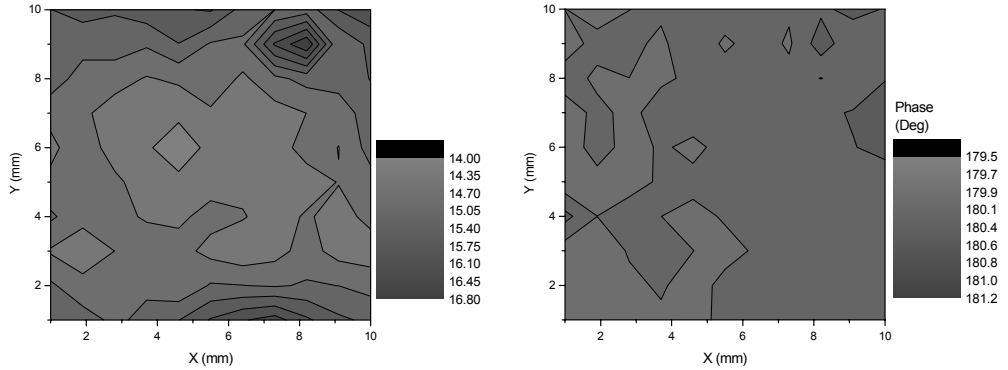

Figure 5. PTR surface maps of a homogeneous AISI 1018 steel sample with 10 Hz modulated beam

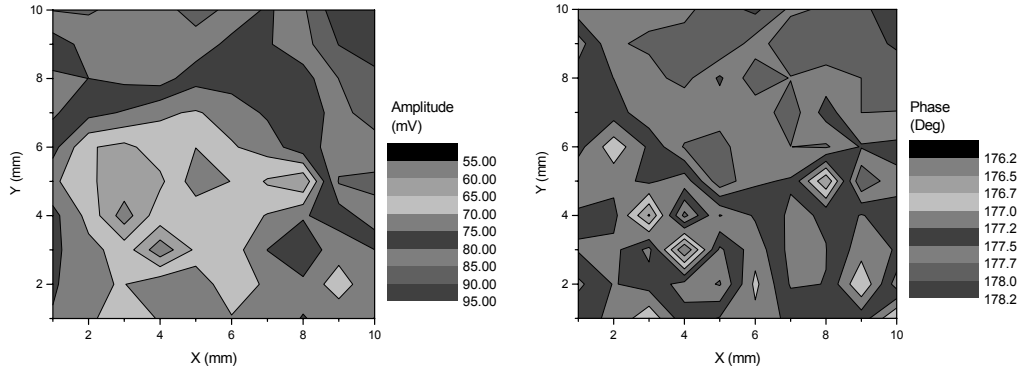

Figure 6. PTR surface maps of a nonhomogeneous AISI 8620 steel sample with 10 Hz modulated beam

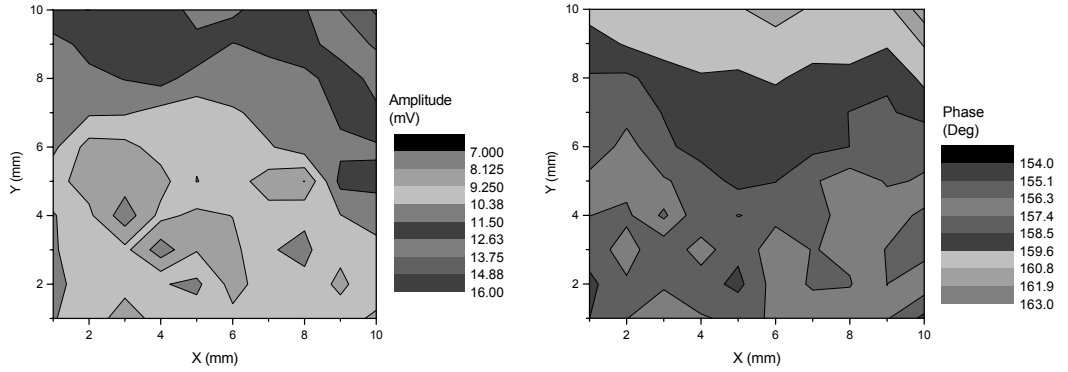

Figure 7. PTR surface maps of a nonhomogeneous AISI 8620 steel sample with 1 kHz modulated beam

of the line scan performed at 10 Hz. This corresponds to a thermal diffusion length of roughly 700 μm, assuming a thermal diffusivity value for the AISI 1018 steel of $1x10^{-5}$ m^2/s (Ref. [9], Table 1, p. 219). There is also a good correlation between the transverse hardness test performed with a 300g load (shallower indentation) and the phase of the line scan at 1000 Hz which probes within a thermal diffusion length of approximately 70 μm. For further evidence of transverse inhomogeneity, a sample was chosen for destructive microhardness depth measurements to be

performed at various locations along the diameter. The results showed that the microhardness at a particular depth is not uniform across the sample, varying as much as 120 HV. Therefore, the sample contains a transverse hardness inhomogeneity, the profile of which is well correlated with the thermophysical inhomogeneity profile imaged by the PTR phase, Fig. 8. In view of the established correlation between thermophysical scan profiles, represented by the thermal-diffusion-length/depth-averaged thermal diffusivity and the hardness scan profiles, Figs. 8 and 9, it can be concluded that the PTR phase images of Figs. 3-7 can be used as hardness images. The changes observed between the low-frequency phase image, Fig. 6, and the high-frequency image, Fig. 7, can therefore be interpreted as variations in hardness profiles, roughly averaged over one thermal diffusion length. As area imaging is too time consuming, a single transverse line scan was introduced, instead, for sample selection. Transverse line-scans performed on each of the carbonitrided and quenched 1018 steel samples at three different frequencies, 10 Hz, 100 Hz and 1000 Hz were employed. At each frequency, the mean and variance of the data sets over the entire amplitude and phase lateral scan were calculated. By use of this line scan method of rejecting the less transversely homogeneous samples, a significant improvement in depth profilometric data inversion was achieved.

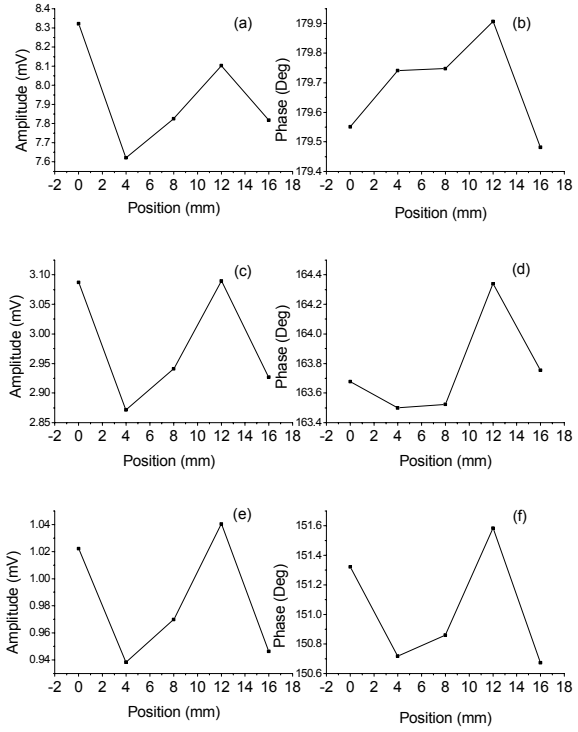

Figure 8. PTR line scan across a particular sample of measured across

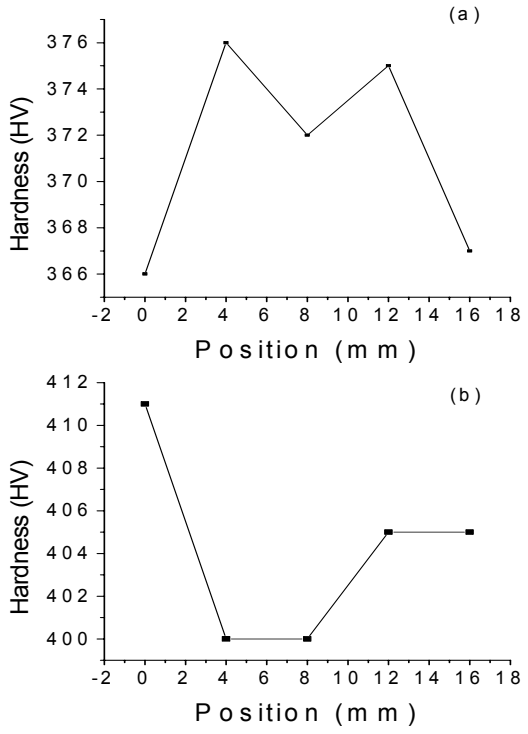

Figure 9. Microhardness test results

AISI 1018 steel: Modulation frequency: a, b –10 Hz the surface of the chosen sample of figure. 8 with
c, d – 100 Hz, e, f – 1 kHz (a) – 1 kg load; and (b) – 300g load.

III. Thermal diffusivity reconstructions: Before any data inversions could be effected it was necessary to select only transversely homogeneous samples for reconstruction as described in sect. II. One dimensional frequency responses of relatively homogeneous samples were used for thermal diffusivity reconstructions. The experimental setup for 1-D frequency scan was similar to the imaging setup. The only difference is that the laser was enlarged to 1.5 cm to guarantee the one-dimensionality of the thermal-wave inverse problem. The thermal diffusivity depth profiles reconstructed from the frequency responses of relatively homogeneous samples and the comparison with hardness profiles are shown in Figures 10 (a) and (b). The error bars represent the standard deviation of the diffusivity depth profiles reconstructed one-by-one from frequency-scan experimental data from all samples with the same nominal case depth.

(a)

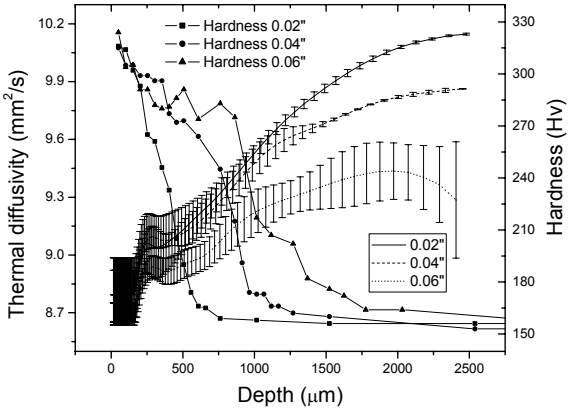

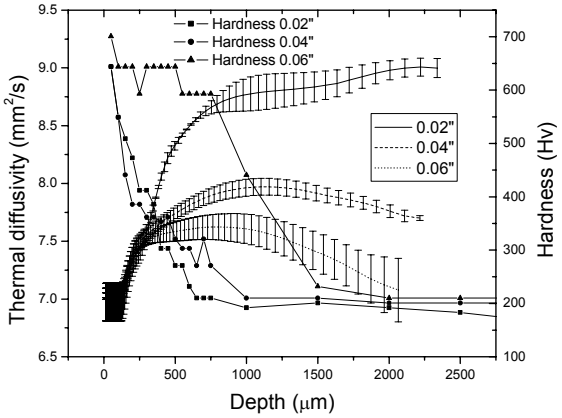

(b)

Figure 10 Thermal diffusivity and hardness as a function of depth coordinate for (a) carbonitrided and (b) quenched AISI 1018 steel samples

Discussion: The present experimental results show that thermal-wave phase hardness scanning imaging at a fixed modulation frequency constitutes a powerful criterion for transverse homogeneity assessment within one thermal diffusion length in hardened steels. Among many

potential uses of such a criterion, from the photothermal point of view it can be applied in selecting suitable candidates for thermal diffusivity and/or conductivity depth profile reconstructions in case hardened steels.

The diffusivity profiles reconstructed from the carbonitrided and quenched samples, exhibit similar behavior. As the carbonitrided curves show, Fig. 10 (a), the thermal diffusivity profile is flat in the near surface area and then increases toward saturation depending. on the hardening case depth. The flatness of the thermal diffusivity curve near the surface region (< 200 μm) is artificial and is directly attributed to the fact that the high frequency portions of the amplitude and phase scans were forced to the normalized values of one and zero, respectively, as part of the roughness elimination methodology. The extent of these flat regions (ca. 200 μm) is indicative of the depth influence of the surface roughness portion on the frequency scans. Compared to the total depth profile of > 2000 μm, the effect of this portion on the diffusivity depth profile is essentially negligible. Overall, the curves can be divided into three sections: flat near-surface section, increasing intermediate-depth section, and flat or slightly changing deep-profile section. The intermediate section of increasing diffusivity can be explained by noting that as the distance from the surface increases the hardness decreases. At depths beyond the diffusion range of the carbon and nitrogen atoms (approximately 500 μm, 1000 μm, 1500 μm for each of 0.02", 0.04" and 0.06" case depths, respectively), the bulk is intuitively expected to remain unchanged during carbonitriding. As a result, the hardness in this region converges to the same value, and the thermal diffusivity should be expected not to change or change slightly. The reconstructed curves of case depth 0.06" further show significant variations resulting in large error bars; nevertheless, the mean value shows a flat or slightly changing thermal diffusivity profile. The diffusivity-hardness anticorrelations are not mirror images of each other and exhibit significant variations for the larger case depths.

As the quenched curves show, Fig. 10(b), the best-reconstructed hardness profile through diffusivity is that corresponding to 0.02" case depth. The inability of the 0.04" and 0.06" diffusivity profiles to reach the level of the 0.02" profile, exhibiting monotonically decreasing saturation and local maxima instead, can be tentatively explained by the variation in bulk thermal diffusivity as a function of case depth heat treating (the treating temperature and time are different for different case depths) and possibly by the breakdown of the assumption of the radial infinite extent of the sample at very low frequencies, leading to lateral thermal-wave confinement. This latter mechanism would also be consistent with the respectively increasing downward bending of the flat portion for the 0.04" and the 0.06" case depth diffusivity profiles in Fig. 10 beyond the 1000 μm range, a feature absent from the 0.02" depth profile. With regard to other features of the reconstructed depth profiles, the mechanical hardness for the carbonitrided samples, Fig. 10 (a), saturates at a level about 160 HV whereas the hardness for the quenched samples, Fig. 10 (b), saturates at a level of about 200 HV. This is in keeping with the expectation that the quenched samples are harder than the carbonitrided samples. Similarly, in keeping with the trend of general anticorrelation between diffusivity and hardness, the overall reconstructed thermal diffusivities of the quenched samples are lower than their corresponding values in the carbonitrided sample.

Conclusions: We have shown that industrial case hardened steel samples often contain thermophysical and mechanical transverse inhomogeneities which are well correlated. By scanning the surface using photothermal radiometry, an image of the mean thermal diffusivity down to a depth fixed by the thermal diffusion length of carbonitrided or otherwise hardened samples can be produced. Phase imaging of hardness inhomogeneities can be used effectively as a criterion for strongly inhomogeneous steels to be excluded from thermal-wave depth-profilometric reconstruction of thermal diffusivity or conductivity. A simple method has been proposed as a quantitative criterion to determine which samples should be chosen or rejected for such thermal-wave reconstructions. Once lateral hardness homogeneity is assured, thermal-wave depth profilometry can be used to further the understanding of the effect of heat treating on AISI

1018 steels subjected to carbonitriding and quenching treatments. Comparison of the reconstructed thermal diffusivity depth profiles of carbonitrided and carbonitrided-quenched samples with the corresponding mechanical hardness depth profiles shows that there is good-to-excellent anti-correlation between hardness and thermal diffusivity profiles for both types of heat-treated samples for case depths up to 0.02", however, the trends deteriorate for deeper case depths, leading to relationships which are not mirror-images. For this particular steel, it appears that both carbon diffusion profiles and the complicated carbonitrided microstructure as well as potential three-dimensional effects due to radial finiteness create dependencies of the bulk values of thermal diffusivity on the heat-treating duration (and thus case depth), which subsequently affect both the absolute values of the thermal diffusivity profiles as well as the depth distribution. Therefore, PTR depth profilometry appears to be a very useful analytical tool in probing this type of case-depth – diffusivity dependencies both in the near-surface regions and in the bulk of heat treated steels with multiple solid-state microstructure phase changes, such as those due to carbonitriding.

References:

[1] J. Jaarinen and M. Luukkala, J. Phys. (Paris) 44, C6-503 (1983).

[2] T. T. N. Lan, U. Seidel, H. G. Walther, G. Goch and B, Schmitz, J. Appl. Phys. 78, 4108 (1995).

[3] M. Munidasa, F. Funak, and A. Mandelis. J. Appl. Phys. 83, 3485 (1998).

[4] A. Mandelis, M. Munidasa, and L. Nicolaides, NDT&E Int. 32, 437 (1999).

[5] D. Fournier, J.P Roger, A. Bellouati, C. Boue, H. Stamm, and F. Lakestani, Anal. Sci. (Japan Soc. Anal. Chem.) 17, s158 (2001).

[6] H. G. Walther, D. Fournier, J. C. Krapez, M. Luukkala, B. Schmitz, C. Sibilia, H. Stamm and J. Thoen, Anal. Sci. (Japan Soc. Anal. Chem.) 17, s165 (2001).

[7] L. Nicolaides, A. Mandelis and C. Beingessner, J. Appl. Phys. 89, 7879 (2001).

[8] G. Busse, Springer Ser. Topics in Current Physics 47, (P.Hess, Ed., Springer-Verlag, Hidelberg, 1989), p. 251.

[9] G. Busse and H.G. Walther, Progress in Photothermal and Photoacoustic Science and Technology, 1, (A. Mandelis, Ed. Elsevier, New York, 1992), Chap. 5.

[10] J. Jaarinen, A. Lehto and M.Luukkala, Proc. IEEE Ultrason. Symp. (B.R. McAvoy, Ed., 1983) p. 659.

[11] G. Busse, Appl. Phys. Lett. 35, 759 (1979).

[12] G. Busse, in Optics in Biomedical Sciences (G. von Bally and P. Greguss, Eds., Springer-Verlag, Berlin 1982), p. 34.

[13] A. Mandelis, Diffusion Wave Fields, Springer, New York (2001), Chap. 5.

References: Text…….